

# Intersubband photoconductivity at 1.6 $\mu\text{m}$ using a strain-compensated AlN/GaN superlattice

E. Baumann, F. R. Giorgetta, and D.<sup>a)</sup>Hofstetter  
*University of Neuchâtel, 1 A.-L. Breguet, Neuchâtel, CH 2000, Switzerland*

H. Lu, X. Chen, W. J. Schaff, and L. F. Eastman  
*415 Phillips Hall, Cornell University, Ithaca, New York 14850*

S. Golka, W. Schrenk, and G. Strasser  
*Institut für Festkörperphysik & Zentrum für Mikro- und Nanostrukturen, Technische Universität Wien, 1040 Vienna, Austria*

We report on intersubband absorption, photovoltaic, and photoconductive detection of near-infrared radiation in regular AlN/GaN superlattice structures. Photoconductive detection was achieved up to temperatures of 120 K. Simulation of the transition energies using a self-consistent Schrödinger-Poisson equation solver for our specific well width is in good agreement with the measurements. For a well width of 17 Å, the transition energy between ground state and first excited state in the GaN well is around 6300  $\text{cm}^{-1}$  which corresponds to 1.6  $\mu\text{m}$ .

Due to its large conduction band discontinuity of around 2 eV and the short intersubband (ISB) lifetime, the AlN/GaN material system is very interesting for high-speed unipolar ISB devices at telecommunication wavelengths around 1.55  $\mu\text{m}$ . The well-established concept of the quantum well infrared photodetector would be the ideal device for such applications.<sup>1</sup> Even though the material quality of nitride compounds is constantly improving, the high dislocation density of  $\sim 10^9 \text{ cm}^{-2}$  is still a limiting factor, especially when it comes to the demonstration of vertical transport based on resonant tunneling. Despite of the small required layer thicknesses, ISB absorption at 1.55  $\mu\text{m}$  and even down to 1.06  $\mu\text{m}$  was already reported from several groups.<sup>2-5</sup> In a different line of research, GaN-based quantum dots embedded in AlN barriers have been explored for ISB devices as well.<sup>6</sup> More recently, we have observed a photovoltaic ISB signal at 1.5  $\mu\text{m}$  in an AlN/GaN superlattice (SL).<sup>7</sup> Although a crude form of vertical transport could be demonstrated in those devices, no photoconductivity in the true sense of the word could be obtained. In this letter, we report on photoconductive and photovoltaic detection of near-infrared radiation at an optical wavelength of 1.6  $\mu\text{m}$  and using two different sample preparations. This wavelength, which corresponds to a transition energy of 800 meV, was confirmed using a self-consistent Schrödinger-Poisson equation solver which calculates the eigenenergies and the difference between the ground state and the first excited state in the quantum well.

The sample was grown by plasma-assisted molecular beam epitaxy on a C-face sapphire substrate. The active layer consists of a 40 period regular SL with silicon doped GaN wells and undoped AlN barriers of the same nominal thicknesses. X-ray and transmission electron microscopy measurements show a SL period of 34 Å. The buffer and cap layers are 540 nm, respectively, 180 nm thick, and consist of fully relaxed, silicon doped 50% AlGaIn. In contrast to our

earlier photovoltaic experiments on samples with an AlN buffer layer,<sup>7</sup> the sample used in this study is strain compensated and thus no conduction band bending is expected under zero-bias conditions. Buffer, cap, and wells are *n*-doped with  $10^{19} \text{ cm}^{-3}$  silicon.

Based on Fermi's golden rule<sup>8</sup> and taking into account a doping density of  $10^{19} \text{ cm}^{-3}$ , a full width at half maximum (FWHM) of  $1700 \text{ cm}^{-1}$ , a peak transition energy of  $6300 \text{ cm}^{-1}$ , and a dipole matrix element  $|\langle n|z|n' \rangle| = 2.2 \text{ Å}$ , an ISB absorption of  $\sim 5\%$  was estimated. The size of this relatively small absorption signal is actually on the same order of magnitude as Fabry-Perot interference fringes and defect-related changes of the sample transmission; it was therefore not possible to obtain an absorption spectrum using the standard multipass waveguide method.

For the photoconductive measurements, the sample was processed into square mesas of 200  $\mu\text{m}$  side length. Mesa fabrication was accomplished using a photoresist mask and Cl:Ar plasma-based reactive ion etching (RIE). The etch depth was  $\sim 600 \text{ nm}$ . Metallic Ti/Al/Ni/Au(10/120/45/50 nm) contacts were evaporated on the top of the mesas and on the etched surface surrounding them (bottom contact). Annealing at 600 °C for 40 s resulted in Ohmic behavior for both top and bottom contacts. The sample was polished to a 45° multipass waveguide and mounted on a copper platelet. For characterization, it was placed into a liquid He flow cryostat and illuminated by the white light source of a Fourier-transform infrared (FTIR) spectrometer. A constant dc bias voltage was applied between top and bottom contact, whereas the occurring small ac current (due to the mirror movement in the FTIR) between those two contacts was amplified and fed back to the FTIR as external detector signal.

No photoconductive signal was measured under zero voltage bias, as expected for a symmetric structure without bending of the conduction band. When applying a small voltage bias of 0.5 V, the amplified current spectrum peaks at  $6300 \text{ cm}^{-1}$  with a FWHM of  $1700 \text{ cm}^{-1}$ . As will be presented in Fig. 3 later, this peak is well fitted by a Lorentzian.

<sup>a)</sup>Electronic mail: fabrizio.giorgetta@unine.ch

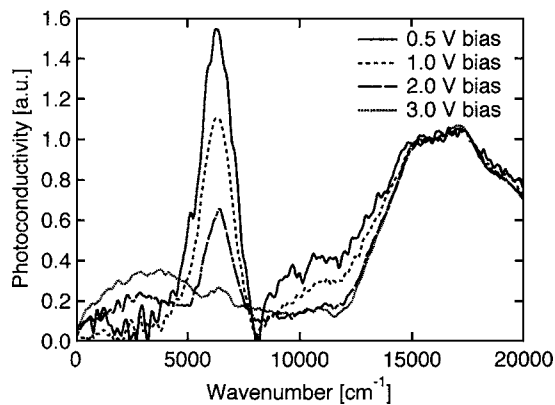


FIG. 1. Bias dependent photoconductive signal measured at 10 K. The feature at  $17\,000\text{ cm}^{-1}$  is due to defects. The ISB signal peaks at  $6300\text{ cm}^{-1}$ .

This signal is due to an increase in conductivity across the SL when electrons are excited from the ground state into the first excited state of the well. Due to the thin barriers, these excited states couple to each other and thus form a miniband. Following the polarity of the applied bias, the photoexcited carriers can be transported vertically via miniband conduction. Due to the conduction band symmetry of the structure, the measured signal is barely affected by the polarity. However, once the voltage drop per period exceeds the width of the miniband, the coupling between the excited states breaks down, and the efficient resonant tunneling conduction is replaced by a much more inefficient hopping-type conduction; this results in a suppression of the photoconductivity peak at  $6300\text{ cm}^{-1}$  which is also shown in Fig. 1. Following the Kronig-Penney model, the width of the first excited state miniband was calculated to be  $60\text{ meV}$ .<sup>9</sup> Considering the total thickness of the SL (40 periods of  $34\text{ \AA}$ ), the electrical breakdown field for the miniband is  $170\text{ kV/cm}$  or  $2.4\text{ V}$  across the whole SL. As Fig. 1 reveals, we observe indeed that the photovoltage signal disappears almost completely when applying  $3\text{ V}$  bias on the structure. A certain voltage drop at the contacts has yet to be taken into account. Due to the relatively large roughness of the underlying AlGaIn buffer layer ( $\text{rms}=10\text{ nm}$ ) and the resulting waviness of the SL, the polarization selection rule is not respected to 100%. We thus observe in this sample an ISB signal in both TE and TM polarization.

The broad photoconductivity peak around  $17\,000\text{ cm}^{-1}$  is due to persistent photoconductivity (PPC) caused by mid-gap defect states.<sup>10</sup> Comparing  $I$ - $V$  curves measured under dark and illuminated conditions we observed that—for any given bias voltage—the conductivity increase due to PPC is proportional to the dark conductivity. Therefore, all spectra in Fig. 1 are normalized according to the current values at the corresponding bias voltage. As expected, this leads to a PPC signal which does not depend on bias.

Figure 2 shows the temperature dependence of the photoconductive signal of the sample processed into mesas. The applied bias was  $0.5\text{ V}$  for all temperatures. The ISB signal peaking at  $6300\text{ cm}^{-1}$  decreases constantly with increasing temperature whereas the PPC signal around  $17\,000\text{ cm}^{-1}$  is maximal around  $120\text{ K}$ . This behavior can be explained by the influence of the PPC on the free carrier density in the SL wells. When excited by optical radiation, the PPC related midgap defects release electrons to the conduction band where they show up as increased  $n$ -type doping concentra-

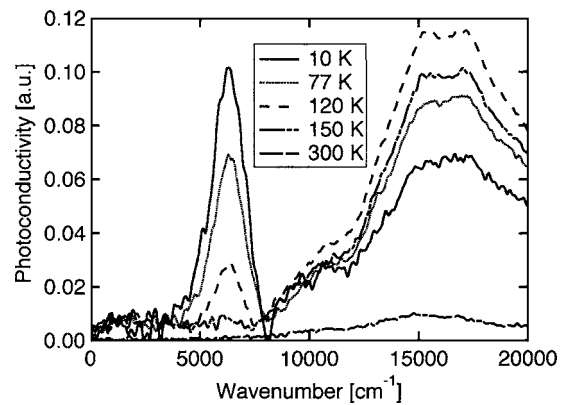


FIG. 2. Temperature dependence of the photoconductive signal. The applied bias is always  $0.5\text{ V}$ . The ISB signal disappears at temperatures higher than  $120\text{ K}$ .

tion. For temperatures below  $150\text{ K}$ , this process results in a new lattice configuration which is metastable. Therefore a certain thermal energy is necessary for the traps to recapture their released electrons. With increasing temperature, the trap recombination rate increases and the actual free carrier density in the wells decreases, leading first to a lower ISB signal and ultimately also to a lower PPC signal. As we will see later, a similar temperature dependence was measured for the photovoltaic sample, where the ISB signal vanished as well for temperatures above  $150\text{ K}$ .

For photovoltaic experiments, the top  $130$ – $150\text{ nm}$  of the AlGaIn cap layer were etched off using RIE;  $50\text{ nm}$  of  $\text{SiO}_2$  was deposited subsequently by plasma enhanced chemical vapor deposition. Two parallel stripes of  $7\text{ mm}$  length  $\times 1\text{ mm}$  width in a distance of  $5\text{ mm}$  were etched into this  $\text{SiO}_2$  layer. Cr/Au-based ( $10\text{ nm}/400\text{ nm}$ ) Ohmic contact stripes were then evaporated onto the remaining AlGaIn cap layer. Between these two Ohmic contacts, which were both connected to common ground, a Cr/Au( $10\text{ nm}/400\text{ nm}$ ) contact was evaporated directly on the  $\text{SiO}_2$  thereby providing a Schottky contact. Current-voltage measurements between the Schottky contact on the  $\text{SiO}_2$  and the two Ohmic contacts on the sample cap showed a Schottky-like characteristics. Similar as the photoconductive device, the sample was polished in a  $45^\circ$  multipass waveguide geometry, mounted on a copper platelet, and placed into a liquid He flow cryostat. Illumination was done using the FTIR internal white light source. As in the photoconductive experiment, the voltage between the contacts was amplified and fed back into the FTIR as detector signal.

Under illumination, a photovoltaic signal peaking at  $6350\text{ cm}^{-1}$  with a FWHM of  $1700\text{ cm}^{-1}$  is observed. As shown in Fig. 3, this photovoltaic signal appears almost exactly at the same energy as the photoconductive signal, and it has also an identical shape. This photovoltage originates from a small band bending at the SL/cap interface. The latter is slightly different for the Ohmic and the Schottky contacts.<sup>11</sup> If the conduction band bends upwards, excited electrons in the wells will preferentially tunnel towards the “downhill” direction and thus deplete the two-dimensional electron gas under the illuminated Schottky contact. Only few wells close to the cap layer “feel” the introduced band bending and contribute to the photovoltaic signal. Again, the broad feature at  $17\,000\text{ cm}^{-1}$  is due to PPC. Since there is no preferential direction for the PPC, the ISB photovoltaic sig-

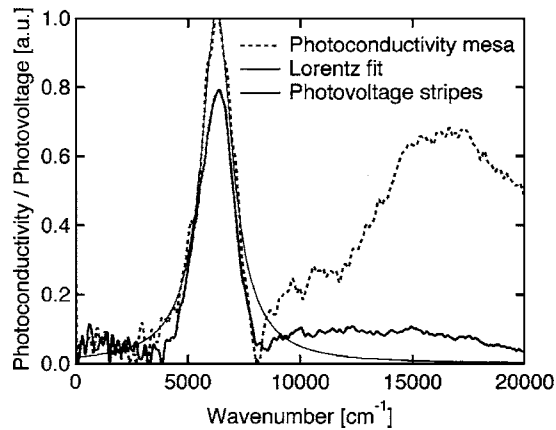


FIG. 3. Comparison of photovoltaic and photoconductive signals at 10 K. A Lorentzian with a peak energy of  $6300 \text{ cm}^{-1}$  and a FWHM of  $1700 \text{ cm}^{-1}$  is fitted to the photoconductivity spectrum.

nal has a much larger amplitude than the PPC signal. In agreement with our earlier publication,<sup>7</sup> the PPC will lead to an improved lateral current flow in the wells and thus to a decreased ISB photovoltage.

The ISB origin of the photoconductive and photovoltaic responses in this structure was further corroborated by characterizing a bulk, silicon doped 50% AlGaIn calibration layer of the same molecular beam epitaxy growth batch as the sample discussed earlier. The calibration sample was prepared for photovoltaic measurement in exactly the same way as the SL sample. The measured photovoltage spectrum shows no signal around  $6300 \text{ cm}^{-1}$ , but a nearly identical PPC signal around  $17000 \text{ cm}^{-1}$ .

In conclusion, we have investigated photoconductive and photovoltaic ISB detection using a regular AlN/GaN SL. The observed signals peaked at  $1.6 \mu\text{m}$  in both cases. For bias voltages larger than 3 V, the photoconductive ISB

signal disappeared; this dependence on bias is in perfect agreement with the computed miniband width of 60 meV. At temperatures above 120 K, no signal could be measured. This effect can be explained by a reduced carrier concentration due to a gradual decay of PPC which provided additional  $n$ -type carriers in the quantum wells.

The authors thank the Professorship Program and the National Center of Competence in Research “Quantum Photonics” both of the Swiss National Science Foundation, the US Office of Naval Research under the NICOP and the MURI programs, as well as the European project NITWAVE (Contract No. 004170) for their generous financial support. For technical assistance, Julien Dorsaz, Pierre Stadelmann, and Daniele Laub (all from EPFL, Lausanne, Switzerland), and Manfred Maier (IAF, Fraunhofer, Freiburg i. Brsg.) are also gratefully acknowledged.

<sup>1</sup>B. F. Levine, *J. Appl. Phys.* **74**, R1 (1993).

<sup>2</sup>C. Gmachl, H. Ng, and A. Cho, *Appl. Phys. Lett.* **79**, 1590 (2001).

<sup>3</sup>D. Hofstetter, S. Schad, H. Wu, W. J. Schaff, and L. F. Eastman, *Appl. Phys. Lett.* **83**, 572 (2003).

<sup>4</sup>A. Helman, M. Tchernycheva, A. Lusson, E. Warde, F. Julien, K. Moutmanis, G. Fishman, E. Monroy, B. Daudin, D. Dang, E. Bellet-Amalri, and D. Jalabert, *Appl. Phys. Lett.* **83**, 5196 (2003).

<sup>5</sup>N. Iizuka, K. Kaneko, and N. Suzuki, *Appl. Phys. Lett.* **81**, 1803 (2002).

<sup>6</sup>M. Tchernycheva, F. Guillot, L. Nevou, E. Monroy, L. Doyennette, A. Helman, R. Colombelli, F. H. Julien, T. Shibata, and M. Tanaka, *Appl. Phys. Lett.* (submitted).

<sup>7</sup>E. Baumann, F. R. Giorgetta, D. Hofstetter, H. Wu, W. J. Schaff, L. F. Eastman, and L. Kirste, *Appl. Phys. Lett.* **86**, 032110 (2005).

<sup>8</sup>M. Helm, *The Basic Physics of Intersubband Transitions, Semiconductors and Semimetals* Vol. 62 (Academic, London, 2000).

<sup>9</sup>G. Bastard, *Wave Mechanics Applied to Semiconductor Heterostructures* (Les Editions de Physique, Les Ulis Cedex, 1988).

<sup>10</sup>V. Ursaki, I. Tiginyanu, P. Ricci, A. Anedda, S. Hubbard, and D. Pavlidis, *J. Appl. Phys.* **94**, 3875 (2003).

<sup>11</sup>T. Cook, C. Fulton, W. Mecouch, R. Davis, G. Lucovsky, and R. Nemanich, *J. Appl. Phys.* **94**, 3949 (2003).